1-9-2021

Autonomous in situ calibration of ion-sensitive field effect transistor pH sensors

Philip J. Bresnahan
University of North Carolina at Wilmington

Yuichiro Takeshita
Monterey Bay Aquarium Research Institute

Taylor Wirth
Scripps Institution of Oceanography

Todd R. Martz
Scripps Institution of Oceanography

Tyler Cyronak
Nova Southeastern University, tcyronak@nova.edu

See next page for additional authors

Find out more information about Nova Southeastern University and the Halmos College of Natural Sciences and Oceanography.
Follow this and additional works at: https://nsuworks.nova.edu/occ_facarticles

Part of the Marine Biology Commons, and the Oceanography and Atmospheric Sciences and Meteorology Commons

NSUWorks Citation

Philip J. Bresnahan, Yuichiro Takeshita, Taylor Wirth, Todd R. Martz, Tyler Cyronak, Rebecca Albright, Kennedy Wolfe, Joseph K. Warren, and Keaton Mertz. 2021. Autonomous in situ calibration of ion-sensitive field effect transistor pH sensors .Limnology and Oceanography Methods : 1 -13. https://nsuworks.nova.edu/occ_facarticles/1145.

Authors

Rebecca Albright
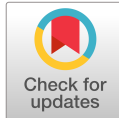*California Academy of Sciences*

Kennedy Wolfe
The University of Queensland

Joseph K. Warren
Monterey Bay Aquarium Research Institute

Keaton Mertz
University of Wisconsin-Madison

Autonomous in situ calibration of ion-sensitive field effect transistor pH sensors

Philip J. Bresnahan [ORCID],[1]* Yuichiro Takeshita,[2] Taylor Wirth,[3] Todd R. Martz,[3] Tyler Cyronak,[4] Rebecca Albright,[5] Kennedy Wolfe,[6] Joseph K. Warren,[2] Keaton Mertz[7]

[1]Department of Earth and Ocean Sciences, University of North Carolina Wilmington, Wilmington, North Carolina
[2]Monterey Bay Aquarium Research Institute, Moss Landing, California
[3]Scripps Institution of Oceanography, University of California San Diego, San Diego, California
[4]Department of Marine and Environmental Sciences, Halmos College of Natural Sciences and Oceanography, Nova Southeastern University, Dania Beach, Florida
[5]California Academy of Sciences, San Francisco, California
[6]Marine Spatial Ecology Lab, School of Biological Sciences, The University of Queensland, St. Lucia, Queensland, Australia
[7]Department of Chemistry, University of Wisconsin-Madison, Madison, Wisconsin

Abstract

Ion-sensitive field effect transistor-based pH sensors have been shown to perform well in high frequency and long-term ocean sampling regimes. The Honeywell Durafet is widely used due to its stability, fast response, and characterization over a large range of oceanic conditions. However, potentiometric pH monitoring is inherently complicated by the fact that the sensors require careful calibration. Offsets in calibration coefficients have been observed when comparing laboratory to field-based calibrations and prior work has led to the recommendation that an in situ calibration be performed based on comparison to discrete samples. Here, we describe our work toward a self-calibration apparatus integrated into a SeapHOx pH, dissolved oxygen, and CTD sensor package. This Self-Calibrating SeapHOx is capable of autonomously recording calibration values from a high quality, traceable, primary reference standard: equimolar tris buffer. The Self-Calibrating SeapHOx's functionality was demonstrated in a 6-d test in a seawater tank at Scripps Institution of Oceanography (La Jolla, California, U.S.A.) and was successfully deployed for 2 weeks on a shallow, coral reef flat (Lizard Island, Australia). During the latter deployment, the tris-based self-calibration using 15 on-board samples exhibited superior reproducibility to the standard spectrophotometric pH-based calibration using > 100 discrete samples. Standard deviations of calibration pH using tris ranged from 0.002 to 0.005 whereas they ranged from 0.006 to 0.009 for the standard spectrophotometric pH-based method; the two independent calibration methods resulted in a mean pH difference of 0.008. We anticipate that the Self-Calibrating SeapHOx will be capable of autonomously providing climate quality pH data, directly linked to a primary seawater pH standard, and with improvements over standard calibration techniques.

Observations of the marine inorganic carbon system and pH in particular have become increasingly common in the past several decades with a sharp rise beginning after the description of ocean acidification (OA; Orr et al. 2005; Fabry et al. 2008; Doney et al. 2009). Of the four master variables—pH, pCO_2, total dissolved inorganic carbon, and total

alkalinity (Millero 2007)—pH is the most commonly measured (and applied) parameter in OA studies, largely due to comparatively high technology readiness levels across a multitude of autonomous pH sensors and analyzers (Seidel et al. 2008; Byrne et al. 2010; Martz et al. 2010, 2015; Wang et al. 2015; Tilbrook et al. 2019). Potentiometric pH sensors utilizing the Honeywell Durafet (Martz et al. 2010), for example, SeaFET and SeapHOx (Bresnahan et al. 2014), have been widely deployed in situ in both moored and mobile applications and have aided in the characterization of variability across both time and space in numerous ecosystems (Hofmann et al. 2011; Frieder et al. 2012; Martz et al. 2014; Takeshita et al. 2015, 2016, 2020*b*; Bresnahan et al. 2016; Johnson et al. 2016, 2017; Rérolle et al. 2016; Williams et al. 2017; Cyronak et al. 2018; Gonski et al. 2018; Saba et al. 2019;

*Correspondence: bresnahanp@uncw.edu

Additional Supporting Information may be found in the online version of this article.

Wright-Fairbanks et al. 2020). However, since Durafet pH sensors require independent calibration based on postdeployment collection of discrete samples (Martz et al. 2010; Bresnahan et al. 2014; McLaughlin et al. 2017) or by making measurements of a known reference pH field at depth (Johnson et al. 2016, 2017) to obtain the highest quality pH measurements, substantial effort is required to ensure accurate, interoperable data from multisensor time series and across multiple research groups. As demonstrated by McLaughlin et al. (2017), operator expertise is currently a key limiting factor in Durafet pH sensor deployments.

Biological impacts of OA are often related to the saturation state of calcium carbonate minerals aragonite or calcite, Ω, a derived variable of the carbonate system (Waldbusser et al. 2015). Consequently, much research has been oriented toward the refinement of estimates of Ω through measurement of several of the four master variables (Newton et al. 2014). Changes in Ω, the product of carbonate and calcium ion concentrations divided by the solubility products of their dominant mineral forms (e.g., aragonite, calcite), are driven primarily by changes in carbonate ion concentration and, therefore, by the inorganic carbon system. As a direct result of the increasing attention given to Ω (and, consequently, on carbonate ion concentration, which can also be measured directly as described in, e.g., Sharp and Byrne 2019), thresholds in uncertainty in the master variables have been prescribed such that carbonate ion concentration and Ω can be estimated with specified degrees of confidence (Newton et al. 2014). In order to observe and monitor processes such as photosynthesis/respiration, calcification/dissolution, and upwelling/downwelling with confidence, carbonate ion concentration should have a relative standard uncertainty of no worse than 10%, and, consequently, pH measurements should have an uncertainty of better than 0.02. However, in order to achieve the "climate" quality goal and observe long-term changes due to OA, these uncertainty thresholds become 1% and 0.003, respectively.

Meeting these stringent thresholds generally requires independent validation of autonomous sensors. For example, pH sensors deployed on Argo floats are routinely validated and adjusted throughout the float's life by referencing their calibration to the deep ocean (Johnson et al. 2017; Claustre et al. 2020) where pH is stable and can be estimated accurately through empirical algorithms (Williams et al. 2016; Bittig et al. 2018; Carter et al. 2018). However, moored pH sensors, particularly in coastal systems, cannot utilize this approach as they cannot periodically measure deep ocean pH. Moored autonomous pH sensors present a challenge in terms of independent validation as they typically require discrete measurements collected in the field near the sensor, typically only collected at the time of deployment and recovery. Spatiotemporal mismatch between sensor and bottle sampling adds to uncertainty in independent validation (Bresnahan et al. 2014; McLaughlin et al. 2017) and a comprehensive discrete sampling program can be painstaking and expensive. Discrete

measurements of the marine inorganic carbon system have been refined for decades (Dickson et al. 2007; Millero 2007; Riebesell et al. 2010); recent work has scrutinized various techniques, uncovering small but measurable effects on pH accuracy from dye impurities as well as a pH-dependent discrepancy between pH measured spectrophotometrically and estimated from total alkalinity and dissolved inorganic carbon measurements (Liu et al. 2011; Carter et al. 2018; Fong and Dickson 2019; Álvarez et al. 2020; Takeshita et al. 2020*a*). All of these issues contribute to increased uncertainty in the pH sensor data and create substantial hurdles in the pursuit of stringent community standards, such as the climate quality goal.

In an alternative approach, in situ validations using traceable standards have been successfully adapted for climate quality pCO$_2$ measurements for moored, underway, and autonomous surface vehicles (Pierrot et al. 2009; Sutton et al. 2014; Chavez et al. 2018; Sabine et al. 2020). A similar method can be adapted for pH sensors using pH standard solutions. Equimolar tris (2-amino-2-hydroxymethyl-1,3-propanediol) in artificial seawater ("tris" hereafter) is considered a primary standard as its pH values are readily traceable to Harned Cell measurements and have been characterized over a range of temperature, pressure, and salinity (Nemzer and Dickson 2005; Rodriguez et al. 2015; Takeshita et al. 2017; Müller et al. 2018; Paulsen and Dickson 2020). Nemzer and Dickson (2005) demonstrated the long-term pH stability of tris buffers when stored in borosilicate glass bottles (< 0.0005 yr^{-1}) and Wolfe et al. (unpubl.) showed an average pH drift of –0.006 yr^{-1} when tris was stored in flexible gas impermeable bags. Tris can therefore serve to independently validate pH measurements in situ, obviating the challenges associated with field sampling and discrete measurement validation approaches. Tris-based validation has been applied to autonomous spectrophotometric pH analyzers (Lai et al. 2018) which are often considered "calibration-free" as pH can be calculated directly and without adjustment (DeGrandpre et al. 1999). However, they have not been applied to potentiometric pH sensors.

This work describes the development and first field test of the Self-Calibrating SeapHOx which utilizes an on-board tris standard to validate autonomous pH measurements periodically throughout a deployment. We seek to improve the quality of Honeywell Durafet pH sensor data sets, in particular measurements made by the SeapHOx, in order to meet climate quality uncertainty criteria. Addition of this capability improves data quality and substantially reduces the efforts required by operators during a field deployment, as they will no longer be required to collect and analyze bottle samples for pH validation. While originally designed for Durafet-based sensors, this technology is readily adaptable to other sensor technologies, provided that those sensors and standards can also be shown to have characterized stability for durations at least as long as their calibration intervals and deployment durations, respectively.

Materials and procedures

Mechanical design

The Self-Calibrating SeapHOx (SCS) is based on the design of the Scripps SeapHOx sensor package comprising pH, dissolved oxygen, and CTD sensors (Bresnahan et al. 2014) with modifications to enable periodic flushing of the measurement cell with a tris standard. pH is measured using the Honeywell Durafet, a combination electrode with an ion-sensitive field effect transistor (ISFET) that responds to hydrogen ion activity and an *internal* Ag/AgCl reference electrode in saturated KCl gel with a liquid junction. A second, *external* junctionless reference electrode, a chloride ion-selective electrode (Cl-ISE), is directly exposed to seawater and allows for a more thermodynamically rigorous calibration and measurement of seawater pH. See Bresnahan et al. (2014) for additional details regarding the differences between the two reference electrodes (and the resulting differences in pH calculations) and the auxiliary sensors.

The SCS utilizes a Sea-Bird Scientific pump (SBE 5P) to pull ambient seawater through a CTD (SBE 37-SI MicroCAT) and deliver it to a flow cell containing the pH sensing components and dissolved oxygen optode (Fig. 1). The SCS modifies the original SeapHOx design with the addition of a three-way valve (International Polymer Solutions M443W1DFS-HT-132) between the CTD and pump. The valve is always open to the flow cell (common port) and can select between (normally open) ambient seawater, pulled through the CTD, or (normally closed) a reservoir of tris buffer in artificial seawater. There are two important consequences of the valve's configuration of normally open to seawater and closed to tris: (1) the valve must be actuated in order to close the valve to ambient seawater and open it to tris, thereby increasing power draw and reducing the instrument's battery life as calibration runs increase and (2) being normally open to seawater means that if the valve were to fail but the remainder of the instrument stay operational, only the calibration functionality would be lost and seawater sampling could otherwise continue as planned. The valve is potted in two epoxy compounds in order to prevent seawater intrusion into the electromechanical components inside its housing: a rigid compound (AeroMarine Products 300/11 Clear Potting and Encapsulation Epoxy Resin) is used on the bottom half of the valve and a flexible compound (AeroMarine 75A Black Underwater Urethane Potting Compound) is used around the cables. The solenoid valve diaphragm is rated to a maximum pressure of 20 dbar. A swing check valve is plumbed into the end of the flow stream on the flow cell outlet to prevent backflushing. Each standardization injection consumes approximately 150 mL of tris.

Tris is stored within a custom, gas impermeable bag based on the design originally utilized in Burke-o-lator pCO$_2$ analyzers (Bandstra et al. 2006) and, subsequently, in an
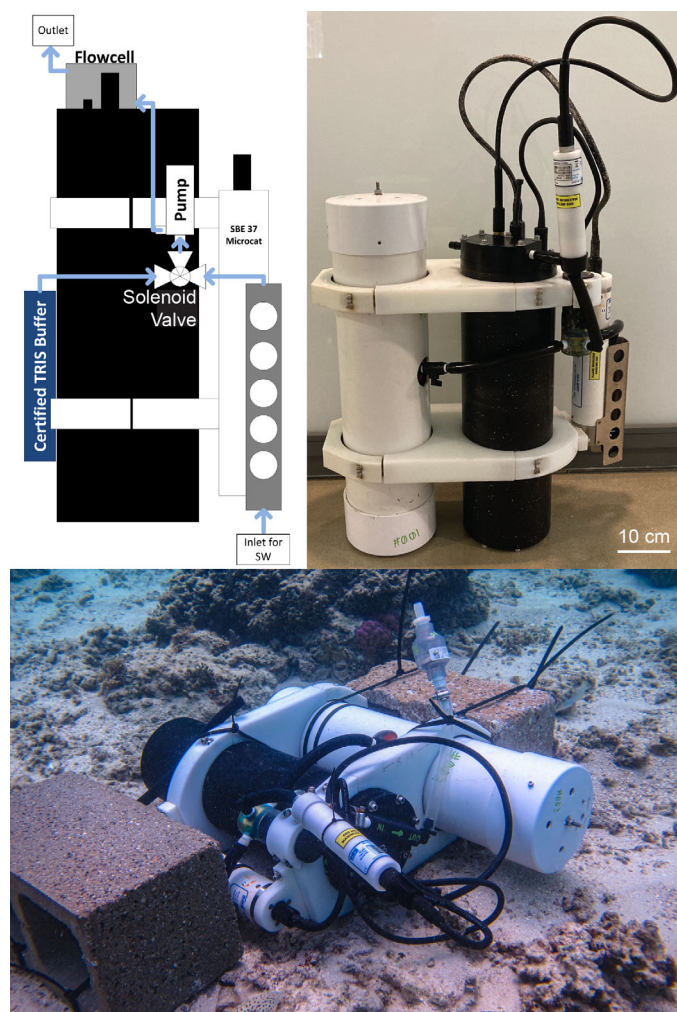

Fig. 1. The self-calibrating SeapHOx assembly. The flow diagram (top left) is labeled for clarity next to a photo (top right) of the fully assembled prototype. (Bottom) Image of SCS deployed on the south reef flat on Lizard Island. The white PVC tube in the photos, represented as a smaller blue rectangle in the flow diagram, contains tris.

evaluation of the stability of tris pH by Wolfe et al. (unpubl.). Briefly, an impermeable film (PAKDRY 7500 barrier film; IMPAK P75C0919) is heat-sealed around its edges with a ball valve fitting to form a closed, approximately 4.5 L reservoir with standard fluidic connectors to integrate it into this design (Hales pers. comm.). The tris reservoir bag is placed within a PVC tube in order to protect it from mechanical damage and to affix it to the SCS. Tris is prepared following Dickson et al. (2007); bromide is added as KBr for a total concentration of 840 μmol L^{-1} due to sensitivity of the Cl-ISE to bromide in seawater (Bresnahan et al. 2014). In the absence of bromide in tris, there is an apparent reconditioning period in externally referenced pH values when toggling between tris and natural seawater which is eliminated through its addition.

There is a critical tradeoff inherent in pump time determination: longer pump times will improve flushing from one measurement to the next which could have a significant impact, especially when switching between ambient seawater and standard, but shorter pump times will minimize reagent usage and power consumption. Additional power is required to open the valve to the standard as well (see details in "Operation" section). Accordingly, the SeapHOx flow cell was iteratively evaluated and redesigned in order to maximize flushing efficiency and minimize flushing volumes required for a $\sim 100\%$ volume replacement from one sample to the next. The flow cell described in prior work (Bresnahan et al. 2014) has an internal volume of 98 mL and substantial dead volume that created issues with flushing. The sensors, especially the Aanderaa oxygen optode 3835/4835, filled much of this volume resulting in an internal fluid volume of 32 mL. The SCS utilizes the Aanderaa optode 5730 which is mounted flush on the surface of the endcap, allowing for a substantial reduction in flow cell height. Accordingly, the SCS flow cell was redesigned to minimize total volume as well as dead volumes utilizing the SOLIDWORKS (Student Premium 2017-18) flow simulation. The Self-Calibrating SeapHOx flow cell total volume is 17 mL total and 16 mL internal fluid volume (i.e., 1 mL is taken up by sensors), signifying a twofold reduction in fluid volume and substantial reduction in dead volume.

Operation

The Self-Calibrating SeapHOx utilizes a custom command line interface to prescribe deployment parameters such as sampling interval (e.g., 30 min). For a typical deployment, during the ambient seawater sampling mode (default), the valve remains unpowered, the pump operates for 10 s, and then the pH, dissolved oxygen, and CTD sensors are sampled. Each recorded pH value (recorded as voltages relative to internal and external reference electrodes— V_{rs}^{int} and V_{rs}^{ext}—see "Analysis" section for further details) is the average of 10 voltage measurements sampled by the custom electronics at 5 Hz. The pump time and sample time amount to roughly 20 s; the instrument subsequently returns to a sleep mode until the next sample.

The command line interface also enables the operator to set calibration frequency (e.g., once per week or, in the case of a 30 min sample period, once every 336 samples). Pump time is identical to that used for ambient seawater samples. The operator has the option to set the number of consecutively repeated calibration replicates in order to improve confidence in flushing and the attainment of a trustworthy calibration value (e.g., following the example above, four consecutive tris calibration runs for every 336 samples).

The SCS was designed to accommodate sufficient reagent and power for 10 months of continuous deployment with monthly calibrations or, alternatively, 10 calibrations at any user-defined calibration frequency. Each calibration as defined here comprises 3–4 consecutive tris injections in order to improve confidence in complete flushing. An additional constraint on calibrations is power: a calibration sample requires almost four times the amount of power of an ambient seawater sample due to the large power draw (~ 13 W) of the valve itself. However, over the course of an extended deployment following the example above (one calibration run/four tris injections every week with ambient sampling at 30 min intervals), the valve accounts for only 1% of the total power budget since the valve is actuated infrequently.

Analysis

The Honeywell Durafet relates pH to a voltage measurement via the Nernst equation,

$$E = E* - \frac{RT_K}{F}\ln(10)*\log_{10}(a_H a_{Cl}), \tag{1}$$

where E is the measured potential, $E*$ represents the reference potential (with junction potentials and other unknown constants lumped in for convenience; Martz et al. 2010), R and F are the universal gas constant and Faraday's constant, T_K is temperature (K), and a is the activity (of H^+ and Cl^-). The term $\log_{10}(a_H a_{Cl})$ can be further broken down to explicitly show the pH term:

$$\log_{10}(a_H a_{Cl}) = \log_{10}(\gamma_H \gamma_{Cl}) + \log_{10}(m_H m_{Cl}) = \log_{10}(\gamma_H \gamma_{Cl} m_{Cl}) - pH \tag{2}$$

where γ is the activity coefficient for the respective ions, and m is molality. $E*$ is the calibration coefficient and has a linear temperature dependency, $\partial E*/\partial T$ (Martz et al. 2010). Once $E*$ and its temperature dependence are known, pH is calculated from voltage, temperature, and salinity measurements.

Following Johnson et al. (2016) and Takeshita et al. (2020a), we transition from the nomenclature above and that which was previously published by this group (Martz et al. 2010; Bresnahan et al. 2014; Takeshita et al. 2014, 2018) to engineering nomenclature which facilitates utilization of a temperature-independent calibration value named k_0. $E*$ is thus redefined here as $k_0 + k_2 \times T_C$, where T_C is temperature in °C, and k_2 is $\partial E*/\partial T$, the calibration coefficient's temperature sensitivity. E is hereafter written as V_{rs}, the reference–source voltage. k_0 is $E*$ at 0°C, and any sensor drift is attributed to changes in k_0. k_2, the calibration coefficient's temperature-sensitivity, is assumed to remain constant as discrete sample vs. Durafet sensor discrepancies have previously been shown not to increase over time as a function of temperature (Johnson et al. 2017). Accordingly, the form of the Nernst equation used hereafter is:

$$V_{rs} = k_0 + k_2*T_C - \frac{RT_K}{F}\ln(10)*\log_{10}(a_H a_{Cl}). \tag{3}$$

The potential for variability in intersensor k_2 values is discussed further in "Comments and recommendations" section. The SeapHOx utilizes two independent pH reference electrodes for redundancy, the so-called internal (as it is physically built into the Honeywell Durafet combination electrode) and external (Cl-ISE, exposed directly to seawater) references. pH^{int} and pH^{ext} are calculated using respective voltages, V_{rs}^{int} and V_{rs}^{ext}, and calibration coefficient pairs, k_0^{int}/k_2^{int} and k_0^{ext}/k_2^{ext}. Auxiliary temperature measurements are required for the calculation of both pH^{int} and pH^{ext}; as the Cl-ISE is sensitive to seawater's halide ion activities, salinity is needed for calculation of pH^{ext}.

The calibration routine determines k_0 at one or more times when V_{rs}, temperature, and, in the case of pH^{ext}, salinity, are measured in a solution of known pH. If multiple k_0 values can be calculated (i.e., multiple calibration samples are available), an average value is used. Previous work (Martz et al. 2010; Bresnahan et al. 2014) suggests that large changes in k_0 during a deployment could be indicative of sensor fouling or failure. Given independent estimates of k_0 throughout a deployment, pH data can be corrected for sensor drift by adjusting k_0 over time. However, in the case of rapid and substantial changes in k_0 due to fouling or sensor failures, data are typically not correctable, though we note that thresholds for acceptable changes have not been formally determined. Barring sensor failure, a commonly observed feature in Durafet and deployments is a conditioning or settling time following deployment due to rehydration of the sensors (1–2 d), exchange with bromide in the case of the Cl-ISE if the sensor was not properly conditioned to seawater prior to deployment (1–2 weeks), as well as thermal equilibration of the sensor housing (hours) (Bresnahan et al. 2014). Adjusting for this drift requires at least one validation point, typically after several days or weeks of continuous operation, making in situ calibration for remote deployments particularly challenging where sample collection after deployment is difficult. We use previously reported average k_2 values (updated from Martz et al. 2010) of $k_2^{int} = 1.25 \, mV/^\circ C$ and $k_2^{ext} = 1.081 \, mV/^\circ C$.

Analysis was performed using Python 3 and PyCO2SYS 1.2.1 for inorganic carbon system calculations (Lewis and Wallace 1998; van Heuven et al. 2011; Humphreys et al. 2020), the TEOS-10 Gibbs Seawater package, gsw (McDougall and Barker 2011), for thermodynamic equation of state calculations (e.g., calculating seawater density from measured salinity and temperature), and pandas, numpy, matplotlib, and seaborn for numerical and plotting routines. CO_2 system calculations use equilibrium constants from Lueker et al. (2000) and assume zero nutrient concentrations. All pH values are reported on the total scale at in situ conditions.

Evaluation: Test tank

A prototype SCS was deployed at 1 m depth in a 5000 L sterilized seawater test tank at Scripps Institution of Oceanography, La Jolla, California, for 6 d in May 2019 in order to demonstrate the self-calibration functionality. To rapidly prove the engineering concept, the standard reservoir was filled with acidified seawater rather than tris. The use of acidified seawater amplified the difference between ambient and standard pH values, enabling a more careful evaluation of the extent of the flow cell's flushing (i.e., if the cell were flushed less than 100%, a larger ΔpH would cause this issue to emerge further beyond the noise of the sensor). The instrument logged ambient conditions at 15 min intervals and performed five consecutive standardization runs every 2 d using the acidified seawater, consuming roughly 150 mL per injection or 750 mL each standardization period.

Evaluation: Field deployment

The SCS was deployed between 26 October 2019 and 10 November 2019, on the South reef flat on Lizard Island, located in the northern part of the Great Barrier Reef (Fig. 1). During this time of year, persistent trade winds induce a predominantly unidirectional wave-driven flow across the reef flat (Silverman et al. 2014), and reef metabolism induces repeatable diel cycles in pH (Pisapia et al. 2019). Sensor readings were made every 5 min, and automated in situ calibrations were conducted every 4 d. Each calibration consisted of four consecutive measurements of tris for a total consumption of approximately 600 mL tris every 4 d. Tris pH was calculated at in situ
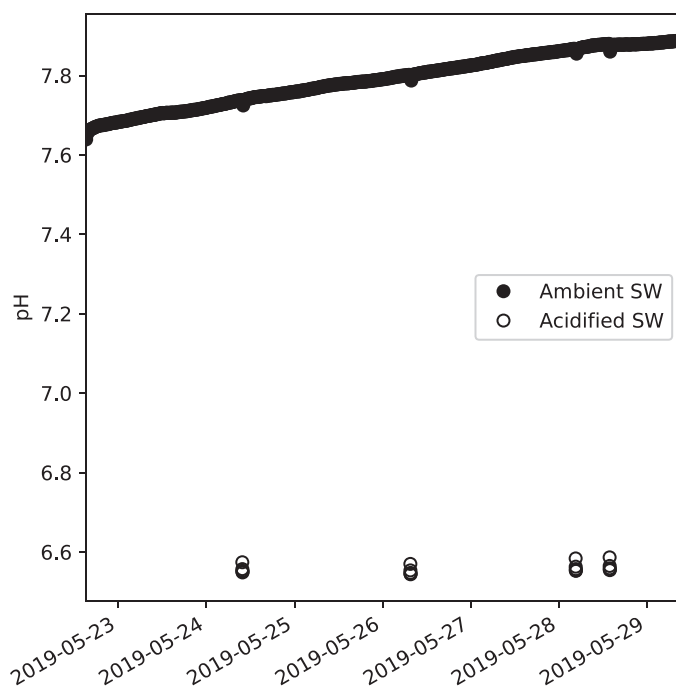

Fig. 2. Six-day time-series in a 5000 L seawater test tank using acidified, sterilized seawater as a reference material. Closed circles represent ambient tank seawater; open represent acidified seawater in standard bag. Note that each cluster of standardization runs comprises five individual consecutive runs.

temperature following eq. 18 in DelValls and Dickson (1998). Water depth was 1.6 ± 0.56 m (mean ± standard deviation [SD]). The SCS was "preconditioned" in the seawater test tank and stored with the electrodes wet and with brominated tris prior to deployment, thereby minimizing conditioning at the beginning of this deployment (Bresnahan et al. 2014).

Discrete samples for pH and total alkalinity were collected every 2 h using an autosampler based on the designs from Albright et al. (2013) and Mucciarone et al. (unpubl.) for a total of 174 samples. For each sample, approximately 500 mL of seawater was pumped into prepoisoned Tedlar bags over 120 s. Bags were purchased from Zefon (P/N: EG-ZP-05EA) and poisoned with saturated $HgCl_2$. Bags were retrieved

and replaced daily. Samples for pH were analyzed spectrophotometrically at 20°C using an automated system based on the design from Carter et al. (2013) and purified meta-cresol purple dye (Liu et al. 2011) from Robert Byrne, University of South Florida. TA was analyzed using an automated titrator (Metrohm 855), as previously described (Albright et al. 2018). pH was adjusted to in situ temperature using PyCO2SYS.

k_0 calibration coefficients for the internal and external reference electrodes were calculated for each discrete sample using spectrophotometry ($k_0^{int,spec}$, $k_0^{ext,spec}$), and for each injection of the on-board tris standard ($k_0^{int,tris}$, $k_0^{ext,tris}$). The first injection of tris for the deployment was removed, as it was contaminated with seawater in the tubing when the tris
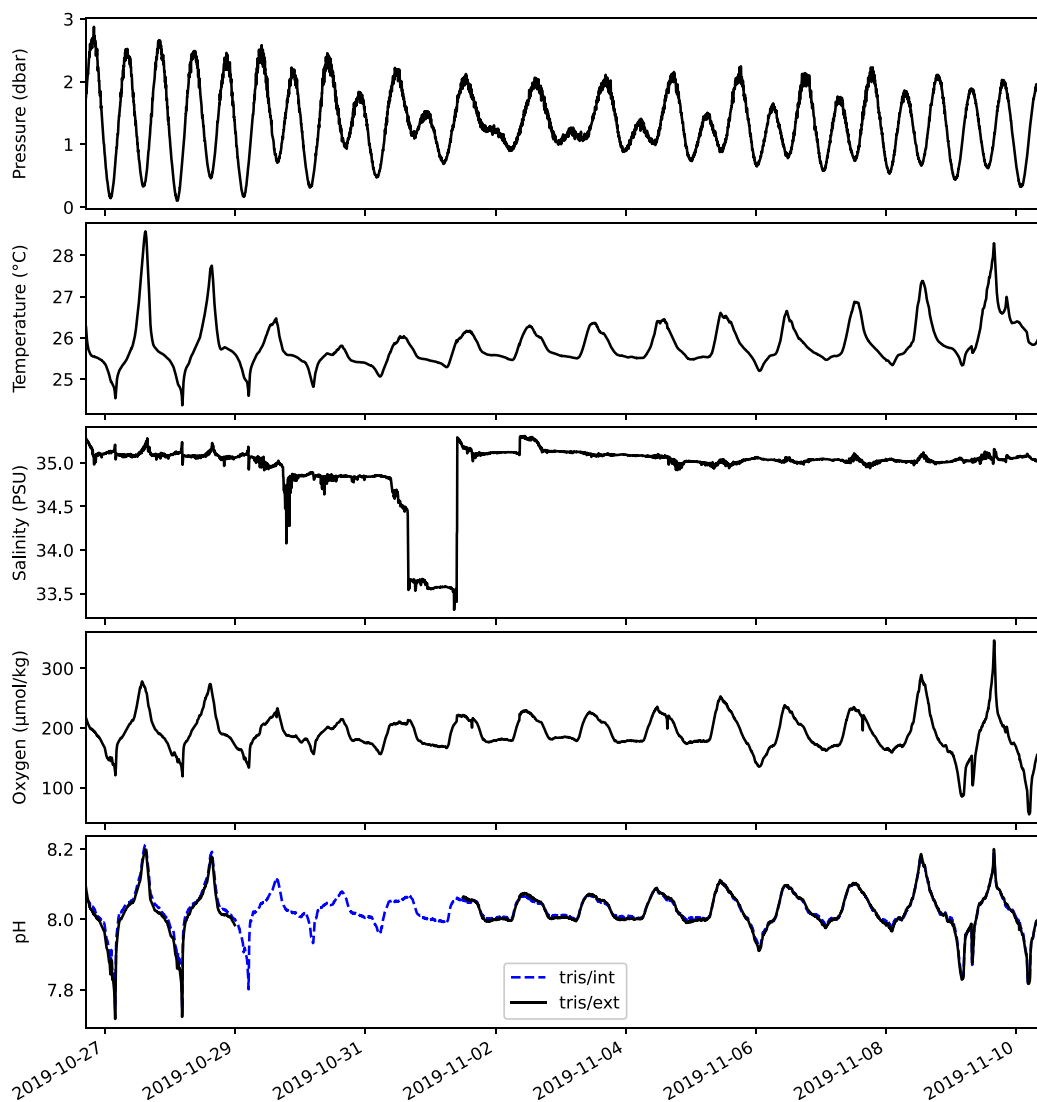

Fig. 3. Pressure (dbar), temperature (°C), salinity (PSU), dissolved oxygen (μmol kg^{-1}), and pH (blue dashed line: pH^{int}, tris-based calibration; black line: pH^{ext}, tris-based calibration) for a 14-d SCS prototype deployment on the south reef on Lizard Island. The salinity time-series illustrates an issue with a partial clog of the CTD beginning 30 October 2019 and cleaned midday on 01 November 2019 after the visible clog was detected; pH^{ext} data are removed during this time. pH is detailed further by calibration methodology in Fig. 4.

Table 1. Number of calibration samples, resulting k_0 values for internally and externally referenced pH when tris and auto-sampler/discrete spectrophotometric pH samples are used for calibration, resulting uncertainty in pH, and n_{95}, the number of requisite calibration samples to achieve climate quality uncertainty.

Calibration/reference	n	k_0 (V, mean ± SD)	pH (SD)	n_{95}
Tris/int	15	−0.363925 ± 0.000280	0.005	9
Tris/ext	15	−1.461604 ± 0.000105	0.002	2
Spec/int	167	−0.363296 ± 0.000370	0.006	17
Spec/ext	127	−1.461134 ± 0.000529	0.009	35

reservoir was connected underwater. Outliers, defined as points more than two SDs from the mean, were removed, resulting in the removal of seven $k_0^{int,spec}$, four $k_0^{ext,spec}$, and zero $k_0^{int,tris}$ or $k_0^{ext,tris}$ values. An average value was calculated from each of these four k_0 time-series, applied to the entire respective sensor time-series (as opposed to a step-wise resetting of k_0), and pH was calculated accordingly (pH^{int,spec}, pH^{ext,spec}, pH^{int,tris}, pH^{ext,tris}). The pH time-series and their k_0 values are compared.

We also calculated the number of calibration samples that would be required for the 95% confidence interval to be smaller than the prescribed climate quality uncertainty of ± 0.003. We used the confidence interval (CI) formula.

$$CI = \pm z \frac{s}{\sqrt{n}}, \qquad (4)$$

rearranged to solve for n (rounding up in order to take the conservative solution), and named the solution n_{95}. CI is

0.003 (the climate quality uncertainty) and z for a 95% confidence interval is 1.96, assuming a normal distribution. s, the SD in calibration pH, is calculated using the SD of each k_0 time-series (s_{k_0}, units of volts) and converted from voltage to pH units using a Nernst slope, or $\frac{RT_K}{F}\ln(10)$, at 25°C of −0.059 V/pH unit. Consequently, we solved for n_{95} as follows:

$$n_{95} = \text{ceiling}\left(\left(1.96 * s_{k_0}/0.059V/0.003\right)^2\right). \qquad (5)$$

We note that this simplified calculation is intended for illustrative purposes only as it assumes that all uncertainty results from the variance in measurement of chosen reference standard and ignores uncertainty in spectrophotometric pH measurement and tris preparation/storage. Analysis code from the Lizard Island deployment is available at https://github.com/SUPScientist/SCS_Analysis.

Assessment

Test tank

Results from the 6-d test tank deployment depict the functionality of the self-calibration mechanism and the effective toggling between two unique sample sources with vastly different pH values (Fig. 2). Figure 2 illustrates a typical calibration routine wherein ambient seawater samples were measured regularly (every 15 min) and standards are measured at longer intervals (> 12 h). Five consecutive standard values were recorded at each simulated calibration interval, enabling a careful evaluation of the extent of flushing of the flow cell. This test deployment clearly demonstrated the ability of the SCS to toggle between two distinct inlets, and to hold "calibration" solution in the flow cell without contamination from ambient seawater. However, multiple injections were required
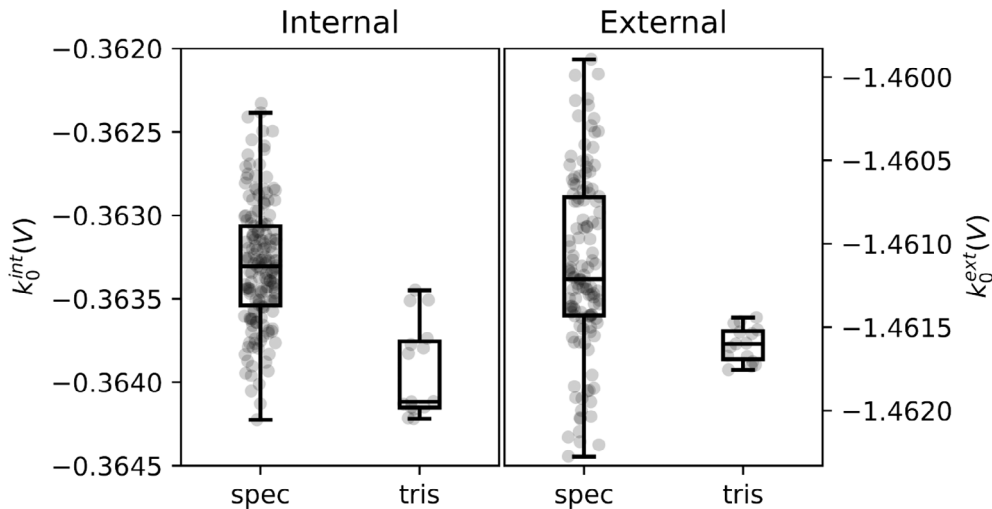

Fig. 4. Box and whisker plots of k_0 values for internal (left panel) and external (right) reference electrodes calculated using calibration values from autosampler (spec) and on-board tris standard (tris). Shaded dots illustrate each calculated value throughout the deployment with a small amount of jitter added to the horizontal axis for clarity. The y-axis range of both panels is 0.0025 V, corresponding to a pH range of 0.042.

to fully flush the flow cell, illustrated in Supporting Information Fig. S2 as the exponential decay of pH as each standardization procedure progressed. The flow cell was redesigned after this evaluation and prior to the Lizard Island deployment in order to improve flushing efficiency and decrease residence time (confirmed via flow simulations in SOLIDWORKS). This test demonstrates the ability for the SCS to measure water from two unique sample sources.

Lizard Island

Data from the SCS deployment at Lizard Island were calibrated two ways: (1) using the integrated tris buffer solution, and (2) to discrete spectrophotometric pH samples. Consistent calibration was achieved across the four tris sample periods during the 2-week deployment on Lizard Island. Each calibration comprised four tris injections, for a total of 16 measurements, and the first injection of the deployment was rejected due to seawater contamination that occurred when connecting the tris reservoir to the sensor underwater ($n = 15$). $k_0^{ext,tris}$ was -1.461604 ± 0.000105 V (mean $\pm$ SD) and $k_0^{int,tris}$ was -0.363925 ± 0.000280 V. This variability approximately translates to SDs of 0.002 and 0.005 in pH, respectively. This excellent reproducibility was obtained in a highly variable environment over a full fortnightly tidal range with large diel ranges in seawater temperature ($>3^\circ$C), oxygen (200 μmol kg^{-1}), and pH (0.4) (Fig. 3). The CTD on the SCS became clogged late on 29 October and was cleaned on 01 November, apparent in the large step changes in salinity (Fig. 3). The regular periodicity of all other signals (viz., pressure, temperature, dissolved oxygen, and pH) combined with the continued agreement between pH^{int} and discrete spectrophotometric measurements during the fouled period, indicates that the clog impacted only the conductivity cell. However, pH^{ext} is explicitly dependent on salinity and there were offsets in pH compared to discrete spectrophotometric measurements during this time. Thus, pH^{ext} was removed from this portion of the time-series.

In contrast, the calibrations based on spectrophotometric pH measurement of over 100 discrete samples exhibited higher variability: SD of the calibration in terms of pH was 0.006 and 0.009 for internal and external referenced values, respectively ($n = 167$ for internal and $n = 127$ for external). Overall, 40 discrete samples were removed from the external time-series due to the conductivity sensor clog (Fig. 3). In order to achieve confidence intervals in pH smaller than climate quality uncertainty of 0.003 following Eq. 5, 2–9 tris-based calibration samples or 17–35 autosampler spectrophotometric measurements would be required (Table 1). This does not necessarily reflect the true absolute accuracy of the sensor; however, it illustrates the improvement in the reproducibility of k_0 obtained with the self-calibrating function.

Average k_0 values calculated using the previously described approaches (Fig. 4) were applied to the entire data set for the
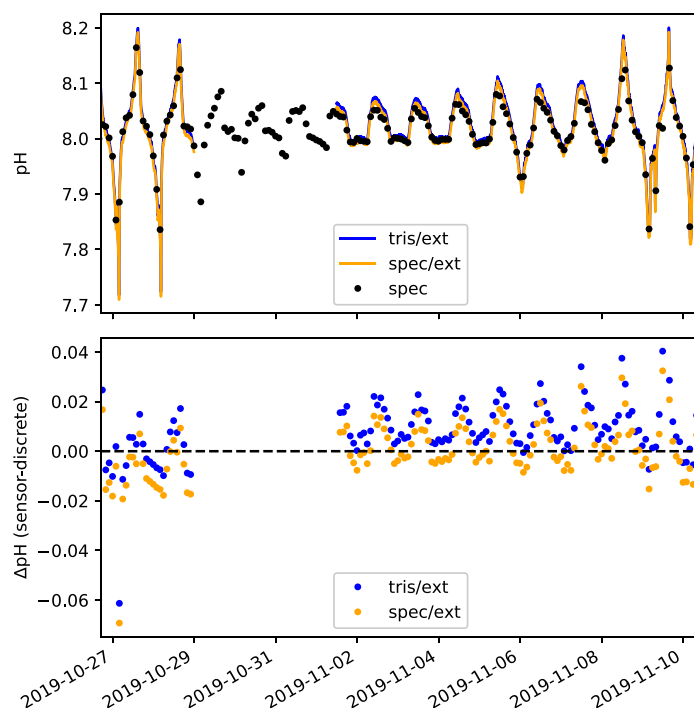

Fig. 5. pH (top) and pH anomaly (bottom) time-series for pH^{ext} when calibrated using tris (novel SCS functionality; blue symbols) or contemporaneous discrete spectrophotometric measurements (traditional calibration technique; orange). The corresponding time-series for pH^{int} and anomalies calibrated using tris and autosampler values were withheld from this figure for improved interpretability and included in Supporting Information.

calculation of pH (Fig. 5). The pH time-series shows good agreement across all methods. The time-series of pH anomalies illustrates both differences in scatter and the mean. By definition of the calibration procedure, the pH calculation based on the spectrophotometric calibration results in an anomaly time-series close to zero. This result is expected since it is a comparison of pH sensor values calibrated using the spectrophotometric values to the spectrophotometric values themselves. Note, however, that this method does not guarantee an anomaly of exactly 0 since k_0 (not pH) is the optimized parameter; variability in temperature (for both pH^{int} and pH^{ext}) and salinity (in the case of pH^{ext}) can lead to small mean anomalies in pH. The independently calculated time-series of pH and pH anomaly for the tris-based calibration are in very close agreement with the spectrophotometric values, reflected in the overlapping uncertainties in k_0: -1.461604 ± 0.000105 V for the tris/ext combination and -1.461134 ± 0.000529 V for the spec/ext combination (mean $\pm$ SD). This 470 μV difference in calculated k_0 values (-1.461134 V $- -1.461604$ V) corresponds to a difference in pH between the two methods of 0.008 using a Nernst slope of -0.059 V/pH unit as described in "Analysis" section. This agreement is particularly remarkable given the independence of the two calibration methodologies.

Discussion

The Self-Calibrating SeapHOx results described here demonstrate important advances in the reduction of uncertainty in autonomous pH measurement. Over the 2-week period at Lizard Island, the SCS was able to obtain repeatable calibration (± 0.002) in a highly variable pH environment. The repeatability of the tris-based calibration was significantly better than that utilizing discrete samples, demonstrating the capacity for this new technology to obtain robust calibrations in situ. However, in addition to the notable differences in the spread of tris vs. spectrophotometrically derived k_0 calculations (i.e., substantially larger SDs for autosampler results), there were small differences in their mean values (pH 0.008). Previous work has demonstrated a discrepancy between spectrophotometric pH measurement and estimation of pH via CO2SYS and measurement of TA/total dissolved inorganic carbon (DIC) (Carter et al. 2018; Fong and Dickson 2019), with a slope of approximately 0.04 and zero difference near pH 7.8. However, Takeshita et al. (2020a) found no systematic discrepancy between spectrophotometric and Durafet measurement of seawater pH indicating that previously measured discrepancies likely stemmed from the combination of variables used in the estimation of the seawater acid-base model in CO2SYS calculations. We attribute our small differences in mean values to tris preparation errors and potential biases in the spectrophotometric measurement. Additionally, as previously described by Bresnahan et al. (2014) and McLaughlin et al. (2017), small spatiotemporal offsets between discrete and autonomous samples can lead to meaningful discrepancies in measurements.

Differences between internally and externally referenced values were due to issues with the conductivity cell, as previously discussed, in addition to what is thought to be a thermal lag in the internal reference gel. While the ISFET itself and the Cl-ISE have reasonably small thermal masses and are directly exposed to ambient seawater, the internal reference electrode is placed in a saturated KCl gel that resides inside the SCS sensor housing. This thermal lag leads to small but significant errors in V_{rs}^{int}, especially when ambient temperature is changing rapidly, as experienced over diel cycles at Lizard Island (> 3°C). For this reason, we choose to show externally referenced values in Figs. 3, 5 and recommend that Durafet-based sensor operators consider the potential impacts of temperature variability on pH^{int}.

The SCS methodology has several meaningful advantages over alternative approaches. pH sensors, especially potentiometric sensors, require careful calibration and validation throughout their deployments typically by comparison to manual discrete samples. The SCS exhibited superior performance in terms of variability when using its self-calibration function in comparison to using contemporaneous discrete samples, ostensibly because it eliminates any error associated with spatiotemporal mismatch during discrete sampling. Where 2–9 calibration samples would be required to achieve better than climate quality

uncertainty via automated tris calibration, roughly 20 discrete samples would be required for spectrophotometric pH-based calibration. Collecting regular discrete measurements throughout a deployment is extraordinarily labor-intensive and, even in what might be considered a best-case scenario of discrete pH measurement every 2 h, the self-calibration function still exhibited superior reproducibility, likely due to spatiotemporal differences and sampling/analytical uncertainties. It is not practical for most autonomous sensor operators to become experts in discrete sample analysis, nor can they afford the ship/lab time required to thoroughly validate sensor measurements in the absence of an integrated validation mechanism. McLaughlin et al. (2017) discovered that the experience level of a Durafet sensor operator played a dominant role in measurement accuracy—a source of uncertainty that can be substantially reduced through autonomous in situ calibration.

There is considerable variability in the quality of spectrophotometric pH measurements between labs (Bockmon and Dickson 2015) and unresolved discrepancies between spectrophotometric pH and pH calculation from TA/DIC (Carter et al. 2018; Fong and Dickson 2019; Álvarez et al. 2020; Takeshita et al. 2020a). There have also been many formulations for the mCP dye used in spectrophotometric pH measurement published recently (Liu et al. 2011; DeGrandpre et al. 2014; Douglas and Byrne 2017; Müller and Rehder 2018); therefore, pH sensors calibrated to spectrophotometric pH may need to be updated in the future if updated constants are published. As the spectrophotometric pH methodology continues to evolve, it becomes increasingly complicated to ascertain what corrections and adjustments (e.g., impure dye corrections, dye perturbation corrections) have been applied to the calibration data and such metadata are not always readily available. On the other hand, if calibration/validation of pH sensors are tied to a traceable standard such as tris, it is much more straightforward to reprocess data and ensure interoperable data moving forward.

Comments and recommendations

The valve diaphragm's pressure rating of 20 dbar currently confines the SCS' utility to the upper 20 m of the surface ocean. The Durafet itself and the standard SeapHOx have a pressure tolerance of 70 dbar (Bresnahan et al. 2014) and the Deep Sea Durafet is operated to 2000 dbar (Johnson et al. 2016). Future work will include incorporation of a Deep Sea Durafet, the pressure-tolerant and calibrated version of the Honeywell Durafet first described by Johnson et al. (2016) and subsequently commercialized by Sea-Bird Scientific. Engineering efforts to pressure-compensate the valve are in progress. Additional work is underway to characterize each sensor's k_2 values which can vary by up to 10% (*unpublished data*) and can lead to significant errors in deployments with high temperature variability. Future deployments will also test the self-

calibration mechanism's longer-term ($\sim$ 9–10 months) deployment capabilities. Continued development will focus on reducing the necessary volume per injection in order to minimize tris requirements; however, a larger tris reservoir could be used for a larger number of calibrations if practical deployment considerations allowed.

A standalone SCS deployment is valuable in its own right for the reasons described above but it could provide multiplicative value in pH sensor networks. For example, if a SCS were deployed near pressure-tolerant and characterized pH sensors included on glider lines (Saba et al. 2019; Takeshita et al. 2020*b*; Wright-Fairbanks et al. 2020), profiling floats (Johnson et al. 2017; Williams et al. 2017, 2018), or fixed profilers such as Wirewalkers (Rainville and Pinkel 2001) or PRAWLERs (Osse et al. 2015; Chu et al. 2020), the SCS could further calibrate or validate those mobile sensor measurements across the whole network. However, as previously discussed, small spatiotemporal offsets between different modes of sampling can lead to challenges with vicarious calibrations.

The inclusion of the valve represents the addition of a single point of failure. As the valve's normally open state keeps it open to ambient seawater and closed to standard, it is highly unlikely that a valve failure would result in the loss of ambient seawater data; however, its diaphragm could become fouled with sediment or biofilm resulting in the potential contamination of both ambient seawater and standard measurements via the leaking of one into the other. The valve, however, is downstream of the Sea-Bird CTD's tributyltin antibiofouling plugs and we do not anticipate that fouling of the internal fluidics will be a significant issue. Moreover, it is possible that in the actuation or release of the diaphragm, small amounts of ambient seawater could seep into the standard bag. The valve actuation could account for a substantial portion of the system's power budget (calibration frequency dependent). We are investigating alternative electronics to minimize the valve's impact on power draw.

Additionally, as has always been the case with potentiometric sensors, the resulting data can be only as good as the sensor's calibration. While we believe that the inclusion of an on-board, traceable standard represents an opportunity for significant improvement of pH data quality and traceability, it also presents opportunities for false security. Certified tris in artificial seawater (i.e., prepared following Dickson et al. 2007 and certified using a Harned Cell) is difficult to procure and in-house preparation following a recipe introduces uncertainties larger than what would be expected from a certified batch (Müller et al. 2018). Importantly, an updated method, described by Paulsen and Dickson (2020), simplifies tris preparation and improves reproducibility. Characterization of tris via spectrophotometric pH measurements is viable, provided that the user follows best practices in order to address the various pitfalls associated with spectrophotometric pH. However, as described in the Introduction, work by Wolfe et al. (unpubl.) quantifies a pH drift of −0.006 yr^{-1} for tris in flexible bags, suggesting the need for measures to eliminate drift (e.g., adding biocide to tris or acid-washing bags prior to filling) or to include this additional source of uncertainty in propagations of error.

In conclusion, we built a prototype Self-Calibrating SeapHOx for high quality, traceable autonomous pH measurement via periodic sampling of an integrated tris buffer in artificial seawater. We deployed the prototype SCS in a seawater test tank for 6 d in order to demonstrate its functionality and subsequently completed a 2-week proof-of-concept study on a coral reef flat on Lizard Island, Australia. The SCS's integrated, autonomous calibration function outperformed a laborious and expensive discrete sampling scheme in terms of repeatability on Lizard Island where large natural variability existed, and demonstrated its potential to provide climate quality pH data with minimal demands on the sensor operator. The SCS has been shown to operate effectively in shallow water with advantages in terms of ease of use, traceability, and reliability in coastal deployments. Future studies will focus on extended and deeper deployments via engineering improvements to the valve's packaging and refinements in the preparation/procurement of tris.

References

Albright, R., C. Langdon, and K. R. N. Anthony. 2013. Dynamics of seawater carbonate chemistry, production, and calcification of a coral reef flat, central Great Barrier Reef. Biogeosciences **10**: 6747–6758. doi:10.5194/bg-10-6747-2013

Albright, R., and others. 2018. Carbon dioxide addition to coral reef waters suppresses net community calcification. Nature **555**: 516–519. doi:10.1038/nature25968

Álvarez, M., N. M. Fajar, B. R. Carter, E. F. Guallart, F. F. Pérez, R. J. Woosley, and A. Murata. 2020. Global ocean spectrophotometric pH assessment: Consistent inconsistencies. Environ. Sci. Technol. **54**: 10977–10988. doi:10.1021/acs.est.9b06932

Bandstra, L., B. Hales, and T. Takahashi. 2006. High-frequency measurements of total CO_2: Method development and first oceanographic observations. Mar. Chem. **100**: 24–38. doi:10.1016/j.marchem.2005.10.009

Bittig, H. C., T. Steinhoff, H. Claustre, B. Fiedler, N. L. Williams, R. Sauzède, A. Körtzinger, and J.-P. Gattuso. 2018. An alternative to static climatologies: Robust estimation of open ocean CO_2 variables and nutrient concentrations from T, S, and O_2 data using Bayesian neural networks. Front. Mar. Sci. **5**:328. doi:10.3389/fmars.2018.00328

Bockmon, E. E., and A. G. Dickson. 2015. An inter-laboratory comparison assessing the quality of seawater carbon dioxide measurements. Mar. Chem. **171**: 36–43. doi:10.1016/j.marchem.2015.02.002

Bresnahan, P. J., T. R. Martz, Y. Takeshita, K. S. Johnson, and M. LaShomb. 2014. Best practices for autonomous

measurement of seawater pH with the Honeywell Durafet. Methods Oceanogr. **9**: 44–60. doi:10.1016/j.mio.2014.08.003

Bresnahan, P. J., and others. 2016. A sensor package for mapping pH and oxygen from mobile platforms. Methods Oceanogr. **17**: 1–13. doi:10.1016/j.mio.2016.04.004

Byrne, R. H., and others. 2010. Sensors and systems for in situ observations of marine carbon dioxide system variables. *In* Proceedings of OceanObs'09: Sustained Ocean Observations and Information for Society. V. 2. ESA Publication WPP-306. doi:10.5270/OceanObs09.cwp.13

Carter, B. R., R. A. Feely, N. L. Williams, A. G. Dickson, M. B. Fong, and Y. Takeshita. 2018. Updated methods for global locally interpolated estimation of alkalinity, pH, and nitrate. Limnol. Oceanogr.: Methods **16**: 119–131. doi:10.1002/lom3.10232

Carter B. R., J. A. Radich, H. L. Doyle, and A. G. Dickson. 2013. An automated system for spectrophotometric seawater pH measurements. Limnology and Oceanography: Methods. **11**: 16–27. doi:10.4319/lom.2013.11.16

Chavez, F. P., J. Sevadjian, C. Wahl, J. Friederich, and G. E. Friederich. 2018. Measurements of pCO$_2$ and pH from an autonomous surface vehicle in a coastal upwelling system. Deep-Sea Res. Part II Top. Stud. Oceanogr. **151**: 137–146. doi:10.1016/j.dsr2.2017.01.001

Chu, S. N., and others. 2020. Field evaluation of a low-powered, profiling pCO$_2$ system in coastal Washington. Limnol. Oceanogr.: Methods **18**: 280–296. doi:10.1002/lom3.10354

Claustre, H., K. S. Johnson, and Y. Takeshita. 2020. Observing the global ocean with biogeochemical-Argo. Ann. Rev. Mar. Sci. **12**: 23–48. doi:10.1146/annurev-marine-010419-010956

Cyronak, T., and others. 2018. Short-term spatial and temporal carbonate chemistry variability in two contrasting seagrass meadows: Implications for pH buffering capacities. Estuaries Coast. **41**: 1282–1296. doi:10.1007/s12237-017-0356-5

DeGrandpre, M. D., M. M. Baehr, and T. R. Hammar. 1999. Calibration-free optical chemical sensors. Anal. Chem. **71**: 1152–1159. doi:10.1021/ac9805955

DeGrandpre, M. D., R. S. Spaulding, J. O. Newton, E. J. Jaqueth, S. E. Hamblock, A. A. Umansky, and K. E. Harris. 2014. Considerations for the measurement of spectrophotometric pH for ocean acidification and other studies. Limnol. Oceanogr.: Methods **12**: 830–839. doi:10.4319/lom.2014.12.830

DelValls, T. A., and A. G. Dickson. 1998. The pH of buffers based on 2-amino-2-hydroxymethyl-1,3-propanediol ('tris') in synthetic sea water. Deep-Sea Res. Part I Oceanogr. Res. Pap. **45**: 1541–1554. doi:10.1016/S0967-0637(98)00019-3

Dickson, A. G., C. L. Sabine, and J. R. Christian [eds.]. 2007. Guide to best practices for ocean CO$_2$ measurements. PICES Special Publication 3, IOCCP Report No. 8., 191 pp., http://cdiac.ornl.gov/oceans/Handbook_2007.html

Doney, S. C., V. J. Fabry, R. A. Feely, and J. A. Kleypas. 2009. Ocean acidification: The other CO$_2$ problem. Ann. Rev. Mar. Sci. **1**: 169–192. doi:10.1146/annurev.marine.010908.163834

Douglas, N. K., and R. H. Byrne. 2017. Achieving accurate spectrophotometric pH measurements using unpurified meta-cresol purple. Mar. Chem. **190**: 66–72. doi:10.1016/j.marchem.2017.02.004

Fabry, V. J., B. A. Seibel, R. A. Feely, and J. C. Orr. 2008. Impacts of ocean acidification on marine fauna and ecosystem processes. ICES J. Mar. Sci. **65**: 414–432. doi:10.1093/icesjms/fsn048

Fong, M. B., and A. G. Dickson. 2019. Insights from GO-SHIP hydrography data into the thermodynamic consistency of CO$_2$ system measurements in seawater. Mar. Chem. **211**: 52–63. doi:10.1016/j.marchem.2019.03.006

Frieder, C. A., S. H. Nam, T. R. Martz, and L. A. Levin. 2012. High temporal and spatial variability of dissolved oxygen and pH in a nearshore California kelp forest. Biogeosciences **9**: 3917–3930. doi:10.5194/bg-9-3917-2012

Gonski, S. F., W.-J. Cai, W. J. Ullman, A. Joesoef, C. R. Main, D. T. Pettay, and T. R. Martz. 2018. Assessment of the suitability of Durafet-based sensors for pH measurement in dynamic estuarine environments. Estuar. Coast. Shelf Sci. **200**: 152–168. doi:10.1016/j.ecss.2017.10.020

Hofmann, G. E., and others. 2011. High-frequency dynamics of ocean pH: A multi-ecosystem comparison. PLoS One **6**: e28983. doi:10.1371/journal.pone.0028983

Humphreys, M. P., L. Gregor, D. Pierrot, S. M. A. C. van Heuven, E. R. Lewis, and D. W. R. Wallace. 2020. PyCO2SYS: Marine carbonate system calculations in Python. doi:10.5281/zenodo.3744275

Johnson, K. S., H. W. Jannasch, L. J. Coletti, V. A. Elrod, T. R. Martz, Y. Takeshita, R. J. Carlson, and J. G. Connery. 2016. Deep-Sea DuraFET: A pressure tolerant pH sensor designed for global sensor networks. Anal. Chem. **88**: 3249–3256. doi:10.1021/acs.analchem.5b04653

Johnson, K. S., and others. 2017. Biogeochemical sensor performance in the SOCCOM profiling float array. J. Geophys. Res. Oceans **122**: 6416–6436. doi:10.1002/2017JC012838

Lai, C.-Z., M. D. DeGrandpre, and R. C. Darlington. 2018. Autonomous optofluidic chemical analyzers for marine applications: Insights from the submersible autonomous moored instruments (SAMI) for pH and pCO$_2$. Front. Mar. Sci. **4**(438): 1–11. doi:10.3389/fmars.2017.00438

Lewis, E., and D. W. R. Wallace. 1998. Program developed for CO$_2$ system calculations. CDIAC-105. Environmental System Science Data Infrastructure for a Virtual Ecosystem.

Liu, X., M. C. Patsavas, and R. H. Byrne. 2011. Purification and characterization of meta-cresol purple for spectrophotometric seawater pH measurements. Environ. Sci. Technol. **45**: 4862–4868. doi:10.1021/es200665d

Lueker, T. J., A. G. Dickson, and C. D. Keeling. 2000. Ocean pCO_2 calculated from dissolved inorganic carbon, alkalinity, and equations for K1 and K2: Validation based on laboratory measurements of CO_2 in gas and seawater at equilibrium. Mar. Chem. **70**: 105–119. doi:10.1016/S0304-4203(00)00022-0

Martz, T., U. Send, M. D. Ohman, Y. Takeshita, P. Bresnahan, H.-. J. Kim, and S. H. Nam. 2014. Dynamic variability of biogeochemical ratios in the Southern California Current System. Geophys. Res. Lett. **41**: 2496–2501. doi:10.1002/2014GL059332

Martz, T. R., J. G. Connery, and K. S. Johnson. 2010. Testing the Honeywell Durafet for seawater pH applications. Limnol. Oceanogr.: Methods **8**: 172–184. doi:10.4319/lom.2010.8.172

Martz, T. R., K. L. Daly, R. H. Byrne, J. H. Stillman, and D. Turk. 2015. Technology for ocean acidification research: Needs and availability. Oceanography **28**: 40–47. doi:10.5670/oceanog.2015.30

McDougall, T. J., and P. M. Barker. 2011. Getting started with TEOS-10 and the Gibbs seawater (GSW) oceanographic toolbox, p. 1–28. SCOR/IAPSO WG 127.

McLaughlin, K., and others. 2017. An evaluation of ISFET sensors for coastal pH monitoring applications. Reg. Stud. Mar. Sci. **12**: 11–18. doi:10.1016/j.rsma.2017.02.008

Millero, F. J. 2007. The marine inorganic carbon cycle. Chem. Rev. **107**: 308–341. doi:10.1021/cr0503557

Müller, J. D., F. Bastkowski, B. Sander, S. Seitz, D. R. Turner, A. G. Dickson, and G. Rehder. 2018. Metrology for pH measurements in brackish waters—part 1: Extending electrochemical pHT measurements of TRIS buffers to salinities 5–20. Front. Mar. Sci. **5**. doi:10.3389/fmars.2018.00176 (176):1–12.

Müller, J. D., and G. Rehder. 2018. Metrology of pH measurements in brackish waters—part 2: Experimental characterization of purified meta-cresol purple for spectrophotometric pHT measurements. Front. Mar. Sci. **5**. doi:10.3389/fmars.2018.00177(177):1–9.

Nemzer, B. V., and A. G. Dickson. 2005. The stability and reproducibility of Tris buffers in synthetic seawater. Mar. Chem. **96**: 237–242. doi:10.1016/j.marchem.2005.01.004

Newton, J., R. A. Feely, E. B. Jewett, P. Williamson, and J. Mathis. 2014. Global ocean acidification observing network: Requirements and governance plan. Second Edition, GOA-ON. http://www.goa-on.org/documents/general/GOA-ON_2nd_edition_final.pdf

Orr, J. C., and others. 2005. Anthropogenic ocean acidification over the twenty-first century and its impact on calcifying organisms. Nature **437**: 681–686. doi:10.1038/nature04095

Osse, T. J., C. Meinig, S. Stalin, and H. Milburn. 2015. The PRAWLER, a vertical profiler powered by wave energy, p. 1–8. *In* OCEANS 2015 - MTS/IEEE Washington.

Paulsen, M.-L., and A. G. Dickson. 2020. Preparation of 2-amino-2-hydroxymethyl-1,3-propanediol (TRIS) pHT buffers in synthetic seawater. Limnol. Oceanogr.: Methods **18**: 504–515. doi:10.1002/lom3.10383

Pierrot, D., and others. 2009. Recommendations for autonomous underway pCO_2 measuring systems and data-reduction routines. Deep-Sea Res. Part II Top. Stud. Oceanogr. **56**: 512–522. doi:10.1016/j.dsr2.2008.12.005

Pisapia, C., E. J. Hochberg, and R. Carpenter. 2019. Multi-decadal change in reef-scale production and calcification associated with recent disturbances on a Lizard Island reef flat. Front. Mar. Sci. **6**(575):1–10. doi:10.3389/fmars.2019.00575

Rainville, L., and R. Pinkel. 2001. Wirewalker: An autonomous wave-powered vertical profiler. J. Atmos. Ocean. Technol. **18**: 1048–1051. doi:10.1175/1520-0426(2001)018<1048:WAAWPV>2.0.CO;2

Rérolle, V., D. Ruiz-Pino, M. Rafizadeh, S. Loucaides, S. Papadimitriou, M. Mowlem, and J. Chen. 2016. Measuring pH in the Arctic Ocean: Colorimetric method or SeaFET? Methods Oceanogr. **17**: 32–49. doi:10.1016/j.mio.2016.05.006

Riebesell, U., V. Fabry, L. Hansson, and J.-P. Gattuso, Luxembourg: Publications Office of the European Union; [eds.]. 2010. Guide to best practices for ocean acidification research and data reporting.1–260.

Rodriguez, C., F. Huang, and F. J. Millero. 2015. The partial molal volume and compressibility of Tris and Tris–HCl in water and 0.725 m NaCl as a function of temperature. Deep-Sea Res. Part I Oceanogr. Res. Pap. **104**: 41–51. doi:10.1016/j.dsr.2015.06.008

Saba, G. K., and others. 2019. The development and validation of a profiling glider deep ISFET-based pH sensor for high resolution observations of coastal and ocean acidification. Front. Mar. Sci. **6**(664):1–17. doi:10.3389/fmars.2019.00664

Sabine, C., and others. 2020. Evaluation of a new carbon dioxide system for autonomous surface vehicles. J. Atmos. Ocean. Technol. **37**: 1305–1317. doi:10.1175/JTECH-D-20-0010.1

Seidel, M. P., M. D. DeGrandpre, and A. G. Dickson. 2008. A sensor for in situ indicator-based measurements of seawater pH. Mar. Chem. **109**: 18–28. doi:10.1016/j.marchem.2007.11.013

Sharp, J. D., and R. H. Byrne. 2019. Carbonate ion concentrations in seawater: Spectrophotometric determination at ambient temperatures and evaluation of propagated calculation uncertainties. Mar. Chem. **209**: 70–80. doi:10.1016/j.marchem.2018.12.001

Silverman, J., and others. 2014. Community calcification in Lizard Island, Great Barrier Reef: A 33-year perspective. Geochim. Cosmochim. Acta **144**: 72–81. doi:10.1016/j.gca.2014.09.011

Sutton, A. J., and others. 2014. A high-frequency atmospheric and seawater pCO_2 data set from 14 open-ocean sites using

a moored autonomous system. Earth Syst. Sci. Data **6**: 353–366. doi:10.5194/essd-6-353-2014

Takeshita, Y., T. R. Martz, K. S. Johnson, and A. G. Dickson. 2014. Characterization of an ion sensitive field effect transistor and chloride ion selective electrodes for pH measurements in seawater. Anal. Chem. **86**: 11189–11195. doi:10.1021/ac502631z

Takeshita, Y., and others. 2015. Including high-frequency variability in coastal ocean acidification projections. Biogeosciences **12**: 5853–5870. doi:10.5194/bg-12-5853-2015

Takeshita, Y., W. McGillis, E. M. Briggs, A. L. Carter, E. M. Donham, T. R. Martz, N. N. Price, and J. E. Smith. 2016. Assessment of net community production and calcification of a coral reef using a boundary layer approach. J. Geophys. Res. Oceans **121**: 5655–5671. doi:10.1002/2016JC011886

Takeshita, Y., T. R. Martz, L. J. Coletti, A. G. Dickson, H. W. Jannasch, and K. S. Johnson. 2017. The effects of pressure on pH of Tris buffer in synthetic seawater. Mar. Chem. **188**: 1–5. doi:10.1016/j.marchem.2016.11.002

Takeshita, Y., K. S. Johnson, T. R. Martz, J. N. Plant, and J. L. Sarmiento. 2018. Assessment of autonomous pH measurements for determining surface seawater partial pressure of CO_2. J. Geophys. Res. Oceans **123**: 4003–4013. doi:10.1029/2017jc013387

Takeshita, Y., K. S. Johnson, L. J. Coletti, H. W. Jannasch, P. M. Walz, and J. K. Warren. 2020a. Assessment of pH dependent errors in spectrophotometric pH measurements of seawater. Mar. Chem. **223**: 103801. doi:10.1016/j.marchem.2020.103801

Takeshita, Y., and others. 2020b. Accurate pH and O_2 measurements from spray underwater gliders. J. Atmos. Ocean. Technol. doi:10.1175/JTECH-D-20-0095.1

Tilbrook, B., and others. 2019. An enhanced ocean acidification observing network: From people to technology to data synthesis and information exchange. Front. Mar. Sci. **6**(337):1–21. doi:10.3389/fmars.2019.00337

van Heuven, S., D. Pierrot, J. W. B. Rae, E. Lewis, and D. W. R. Wallace. 2011. MATLAB program developed for CO_2 system calculations. ORNL/CDIAC-105b. Carbon Dioxide Information Analysis Center, Oak Ridge National Laboratory, U.S. Department of Energy.

Waldbusser, G. G., and others. 2015. Saturation-state sensitivity of marine bivalve larvae to ocean acidification. Nat. Clim. Chang. **5**: 273–280. doi:10.1038/nclimate2479

Wang, Z. A., F. N. Sonnichsen, A. M. Bradley, K. A. Hoering, T. M. Lanagan, S. N. Chu, T. R. Hammar, and R. Camilli. 2015. In situ sensor technology for simultaneous spectrophotometric measurements of seawater total dissolved inorganic carbon and pH. Environ. Sci. Technol. **49**: 4441–4449. doi:10.1021/es504893n

Williams, N. L., and others. 2016. Empirical algorithms to estimate water column pH in the Southern Ocean. Geophys. Res. Lett. **43**: 3415–3422. doi:10.1002/2016GL068539

Williams, N. L., and others. 2017. Calculating surface ocean pCO_2 from biogeochemical Argo floats equipped with pH: An uncertainty analysis. Global Biogeochem. Cycles **31**: 591–604. doi:10.1002/2016GB005541

Williams, N. L., L. W. Juranek, R. A. Feely, J. L. Russell, K. S. Johnson, and B. Hales. 2018. Assessment of the carbonate chemistry seasonal cycles in the Southern Ocean from persistent observational platforms. J. Geophys. Res. Oceans **123**: 4833–4852. doi:10.1029/2017JC012917

Wright-Fairbanks, E. K., T. N. Miles, W.-J. Cai, B. Chen, and G. K. Saba. 2020. Autonomous observation of seasonal carbonate chemistry dynamics in the Mid-Atlantic Bight. J. Geophys. Res. Oceans **125**: e2020JC016505. doi:10.1029/2020JC016505

Acknowledgments

Conflict of Interest

None declared.